NUKLEONIKA 2015;60(3):571–580
doi: 10.1515/nuka-2015-0102

ORIGINAL PAPER

DE GRUYTER
OPEN

Comparative analysis between measured and calculated concentrations of major actinides using destructive assay data from Ohi-2 PWR

Mikołaj Oettingen, Jerzy Cetnar

Abstract. In the paper, we assess the accuracy of the Monte Carlo continuous energy burnup code (MCB) in predicting final concentrations of major actinides in the spent nuclear fuel from commercial PWR. The Ohi-2 PWR irradiation experiment was chosen for the numerical reconstruction due to the availability of the final concentrations for eleven major actinides including five uranium isotopes (U-232, U-234, U-235, U-236, U-238) and six plutonium isotopes (Pu-236, Pu-238, Pu-239, Pu-240, Pu-241, Pu-242). The main results were presented as a calculated-to-experimental ratio (C/E) for measured and calculated final actinide concentrations. The good agreement in the range of ±5% was obtained for 78% C/E factors (43 out of 55). The MCB modeling shows significant improvement compared with the results of previous studies conducted on the Ohi-2 experiment, which proves the reliability and accuracy of the developed methodology.

Key words: comparative analysis • major actinides • MCB • Monte Carlo • pressurized water reactor (PWR)

M. Oettingen✉, J. Cetnar
Department of Nuclear Energy,
Faculty of Energy and Fuels,
AGH University of Science and Technology,
30 Mickiewicza Ave., 30-059 Krakow, Poland,
Tel.: +48 12 617 5186, Fax: +48 12 617 4547,
E-mail: moettin@agh.edu.pl

Received: 24 September 2014
Accepted: 20 May 2015

Introduction

The reliability and safety of the nuclear systems are estimated in the series of numerical simulations performed using various numerical tools. The tools should provide high confidence level to predict system response during normal operation conditions and accident situations. Only by the comparative analysis the quantitative relationship between results of experimental measurements and numerical simulation can be established. On this basis, one can decide if applied numerical tool and associated methodology in a sufficient way reflect reality and might be further used to solve advanced problems related to the nuclear science and engineering. The predictive capabilities of the burnup codes like MCB [1] are essential for the characterization of the nuclear fuel being irradiated in the existing and newly designed nuclear systems (e.g. GEN-IV nuclear reactors). The computed concentrations of major actinides serve further to optimize all steps of the back-end of the nuclear fuel cycle related to the spent fuel treatment before its reprocessing or final disposal. Therefore, applied numerical tools should present high consistency with experimental measurements.

Comparative analysis should rely on the reference measurements obtained in the dedicated experiments. The more experimental design and

operational data are available the more reliable is the numerical reconstruction, and thus the results could be estimated with higher accuracy. Unfortunately, most experiments are performed in scientific nuclear reactors, therefore it does not reflect the reality of the commercial system. Even though some experiments were performed in the commercial reactors, usually the access to the operational parameters is restricted to scientific community. Each outcome of the experiment always depends on the current reactor core loading pattern, which determines the duration of reactor cycle and energy production. This influences the revenue of the utility and thus is treated as confidential information. Additionally, the costly industrial irradiation experiments must always be directly related to the economical profits for the utility. The utilities are mostly interested in the fuel mechanical properties like integrity under irradiation, which plays an important role, e.g., for burnup extension. The knowledge about the final actinide concentrations for the comparative analysis and associated improvement of the numerical tools is seldom desired and in consequence hardly available. The Ohi-2 irradiation experiment was chosen for the comparative analysis due to availability of the measured actinide concentrations and vast set of additional operational and design parameters [2].

Section 'Irradiation' describes the general layout of the Ohi-2 PWR and irradiated fuel assembly. Section 'Samples' shows briefly the experimental procedures deployed for the estimation of final actinide concentrations and sample burnup. In the section 'The MCB code' we present the numerical tool applied for the reconstruction of the Ohi-2 experiment. Section 'Numerical' illustrates the features of the developed numerical model for MCB simulation while the section 'Results' presents scientific outcome of the study. The last section summarizes performed analysis and recommends directions for future research.

Irradiation

The final concentrations of major actinides obtained in the experimental measurements are the reference values for the comparative analysis. The concentrations were attained in the destructive assay of the five spent fuel samples irradiated at Japanese Ohi-2 PWR of the Kansai Electric Power Company Inc. (KEPCO) [3]. The Ohi-2 operates 4-loop Westinghouse PWR with the thermal power of 3424 MW_{th} and efficiency of about 33%. The reactor reached first criticality on December 1979 – nine months after Ohi-1. The inlet coolant temperature equals 289°C while the outlet coolant temperature is 325°C. The water circulates in the primary cooling circuit under pressure of 15.5 MPa. The core contains 193 fuel sub-assemblies of the type 17 × 17 arranged in the square pattern. The equivalent core diameter equals 3.37 m, while the active column height 3.66 m. Figure 1 shows the horizontal cross cut of the core with the most common initial 3-region Out--In checkerboard fuel loading pattern and banks of the rod cluster control assemblies.

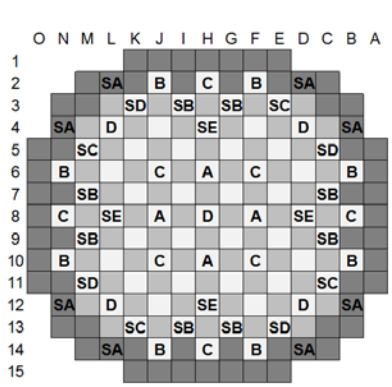

U235 wt%	Nr of FA
2.1	65
2.6	64
3.1	64
Control bank	Nr of clusters
A	4
B	8
C	8
D	5
Shutdown bank	Nr of clusters
SA	8
SB	8
SC	4
SD	4
SE	4

Fig. 1. The initial 3-region Out-In checkerboard loading pattern and banks of the rod cluster control assemblies.

Table 1. Initial isotopic fuel composition

Isotope	Gd_2O_3 + UO_2 [wt%]	UO_2 [wt%]
U-234	0.0141	0.0281
U-235	1.6874	3.2
U-236	0.0008	0.002
U-238	98.2977	96.7699
Gd-152	0.19	NA
Gd-154	2.13	NA
Gd-155	14.58	NA
Gd-156	20.30	NA
Gd-157	15.62	NA
Gd-158	24.95	NA
Gd-160	22.23	NA

The investigated 17 × 17 fuel assembly indexed as 17G encompasses 264 fuel rods containing fissile material in the form of uranium dioxide UO_2. However, only 248 rods contain pure uranium fuel enriched to 3.2 wt% of U-235. The remaining 16 rods contain 6 wt% Gd_2O_3 and 94 wt% UO_2 enriched to 1.7 wt% U-235. The isotopic composition of the applied nuclear fuel is specified in Table 1. The gadolinia burnable absorber provides additional excess reactivity at the beginning of the reactor cycle [4]. This, in turn allows deployment of nuclear fuels with higher enrichment and finally extension of the reactor cycle. In addition, every 17 × 17 FA encloses 24 control rods guiding tubes and one inspection thimble made of zircalloy-4. The 17G FA was irradiated during two following reactor cycles of 410 and 427 EFPD from July 1985 to February 1987. The in-core location of the assembly was changed after interim operational outage of 104 days from peripheral position C13 to inner position E11. The first irradiation cycle corresponds to the 5th general reactor cycle while the second to the 6th general reactor cycle. The fuel assembly was discharged at the average burnup of 31.5 GWd/t. Table 2 summarizes the main parameters of the 17 × 17 PWR fuel assembly.

Samples

The analytical measurements were performed just after the discharge of the leading fuel sub-assembly

Table 2. Specification of the 17 × 17 PWR fuel assembly

Fuel assembly	
Dimensions [mm]	214 × 214
No. of fuel rods	264
Fuel rod pitch [mm]	12.6
No. of guide tubes	24
No. of instrument thimbles	1
Fuel rod	
Rod length [mm]	3852
Active height [mm]	3660
Clad gap [mm]	0.17
Cladding	
Material	Zry-4
Outer diameter [mm]	9.5
Thickness [mm]	0.64
Fuel pellet	
Density [g/cm^3]	10.42*
Diameter [mm]	8.05

* The density in unit g/cm^3 was not reported, only the theoretical density of 0.95% was known.

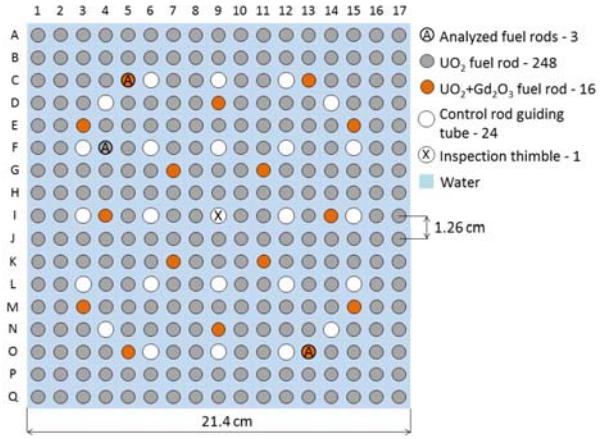

Fig. 2. Horizontal cross cut of the 17G fuel assembly.

from the reactor core at the Japan Atomic Energy Research Institute (JAERI) [5]. Five fuel samples for the destructive assay were cut from the bottom of two Gd_2O_3 + UO_2 fuel rods and one UO_2 fuel rod marked C5, O13 and F4, respectively. Figure 2 shows placement of the investigated fuel rods in the fuel assembly, while Fig. 3 depicts an axial location of the cut fuel samples in the fuel rods. Samples weighed

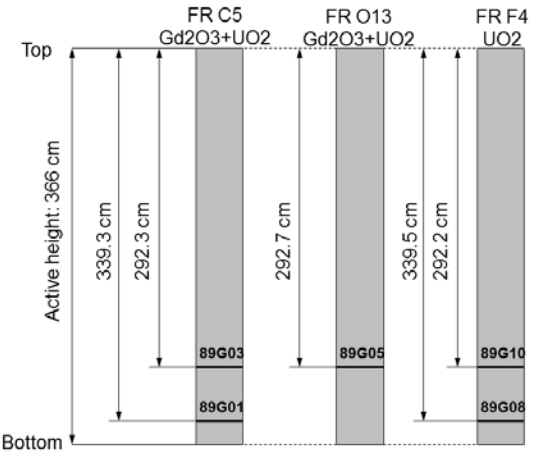

Fig. 3. Cutting position of fuel samples.

about 2 g and had a shape of round slice with thickness of about 3 mm. Each sample was dissolved in the 30 ml of 4 M nitric acid solution at temperature 100°C. Next, the two-step separation process was applied to separate elements of interest for further analysis. Firstly, Pu, U, Np were separated inside the anion exchange column. Secondly, the same anion exchange column was applied to extract fractions of Nd, Am and Cm from the remaining material. Lastly, the mass spectrometry and alpha spectrometry techniques were applied to measure final concentrations of isotopes. The results were finally presented in unit g/tIHM – gram per ton of initial heavy metal [6]. Table 3 presents measured concentrations of major actinides obtained in post-irradiation assay while Table 4 associated measurement errors.

The measured actinide concentrations are necessary to quantify sample burnup. The burnup is the measure of the integral local energy released by the nuclear fuel during irradiation and is usually reported in the unit GWd/tIHM[1)]. Numerically, it might be estimated using the recoverable energy per fission for all fissionable nuclides in the nuclear fuel. However, the definition of the recoverable energy per fission depends on the linked nuclear data libraries and physical models implemented in the numerical tool. This, in turn may result in the same burnup values for different number of fissions and following

[1)] Gigawatt-day per ton initial heavy metal.

Table 3. Measured concentrations of major actinides [2]

Actinide	Measured concentration [g/tIHM]				
	89G01	89G03	89G05	89G08	89G10
U-232	1.26E-03	1.76E-03	1.53E-03	3.26E-04	4.02E-04
U-234	8.75E+01	7.47E+01	8.13E+01	1.71E+02	1.48E+02
U-235	5.47E+03	3.65E+03	4.42E+03	9.10E+03	6.12E+03
U-236	1.97E+03	2.23E+03	2.14E+03	3.84E+03	4.24E+03
U-238	9.60E+05	9.53E+05	9.56E+05	9.45E+05	9.38E+05
Pu-236	3.78E-04	7.21E-04	5.72E-04	7.22E-04	1.32E-03
Pu-238	6.82E+01	1.21E+02	9.35E+01	1.11E+02	1.90E+02
Pu-239 + Np-239	5.36E+03	5.51E+03	5.52E+03	5.18E+03	5.32E+03
Pu-240	2.15E+03	2.61E+03	2.42E+03	2.15E+03	2.61E+03
Pu-241	1.24E+03	1.55E+03	1.43E+03	1.21E+03	1.49E+03
Pu-242	4.28E+02	7.58E+02	6.05E+02	4.37E+02	7.51E+02

Table 4. Measurement error of major actinides [2]

Actinide	Measurement error [%]				
	89G01	89G03	89G05	89G08	89G10
U-232	1.6	2.2	2.5	6.9	11.0
U-234	1.1	1.3	1.0	1.1	1.3
U-235	<0.5	<0.5	<0.5	<0.5	<0.5
U-236	<0.5	<0.5	<0.5	<0.5	<0.5
U-238	<0.5	<0.5	<0.5	<0.5	<0.5
Pu-236	3.1	3.3	3.1	3.8	4.5
Pu-238	0.6	6.6	0.5	0.9	1.6
Pu-239 + Np-239	<0.5	<0.5	<0.5	<0.5	<0.5
Pu-240	<0.5	<0.5	<0.5	<0.5	<0.5
Pu-241	<0.5	<0.5	<0.5	<0.5	<0.5
Pu-242	<0.5	<0.5	<0.5	<0.5	<0.5

Table 5. Burnup of the spent fuel samples obtained using Nd-148 method [2]

Sample	89G01	89G03	89G05	89G08	89G10
Burnup FIMA [%]	2.211	2.950	2.585	3.129	3.980

inconsistencies in final isotopic fuel composition. Therefore, the usage of aforementioned burnup definition is not recommended and the new FIMA[2)] unit was introduced. The FIMA unit indicates the decrement of heavy metal during irradiation and is commonly used for normalization of the burnup calculations. The reference burnup in FIMA unit was experimentally estimated at JAERI using the Nd-148 method defined in ASTM E321 – 96(2012) [7]. The values obtained for all five fuel samples were further used for the normalization of MCB calculation – see Table 5.

The MCB code

The Monte Carlo continuous energy burnup code – MCB is the general numerical tool dedicated for neutron transport and burnup calculations. The code is under constant development at the Department of Nuclear Energy of AGH University of Science and Technology, Krakow, Poland and was successfully applied in six EURATOM projects for nuclear reactor core design and optimization:

- PDS-XADS – Preliminary Design Studies of an Experimental Accelerator-driven System (2001–2004),
- EUROTRANS – European Research Programme for the Transmutation of High Level Nuclear Waste in an Accelerator Driven System (2005–2009),
- PUMA – Plutonium and Minor Actinides Management in Thermal High Temperature Reactors (2006–2009),
- ELSY – European Lead-cooled System (2006–2009),
- LEADER – Lead-cooled European Advanced Demonstration Reactor (2010–2013),
- FREYA – Fast Reactor Experiments for Hybrid Applications (2011–ongoing).

[2)] Fission per initial metal atom.

The development of MCB aims creation of the multiphysics tool able to provide accurate description of the complex nuclear systems like nuclear power reactors of the III, III+ and IV Generation. The comparative analysis is the next significant step in the long-term process leading up to the final acceptance of the MCB code by the scientific community as a reliable tool for commercial applications.

From the technical point of view, MCB integrates the commercial Monte Carlo transport code: A general Monte Carlo n-particle transport code (MCNP) [8] and the novel transmutation trajectory analysis code (TTA) [1]. The MCNP subroutines are used for neutron transport simulation, while TTA automatically forms and analyses transmutation and decay chains for nuclide density evolution in time function. The calculation of the nuclide density time evolution is performed in two processing steps. First, at the beginning of the arbitrary time step, MCB calculates contribution to neutron spectra from every sampled particle in the selected geometrical regions of the numerical model called fuel zones. On this basis, the decay and reaction probabilities for every possible channel are assigned and associated reaction rates are calculated. Second, the code automatically forms material composition obtained from the time depended transmutation and decay chains. Next, through the decomposition of the nonlinear transmutation trajectories into the series of the linear chains, the transmutation trajectory generator [9] allows to reflect mathematically the Bateman equations. The formed Bateman equations are solved using the linear chain method, which results in new nuclide densities at the end of the arbitrary time step [9]. Next, neutron spectra for new nuclide densities are calculated and new decay and reaction probabilities are assigned. The whole process is repeated for all given time steps. At the end of calculations, user obtains final nuclide densities and supplementary parameters like: neutron flux, neutron multiplication factor, decay heat, reaction rates, material activity, potential dose and many others.

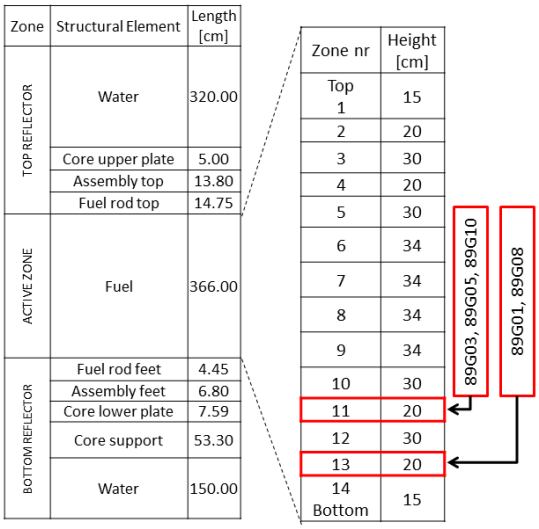

Fig. 4. Vertical cross cut of the numerical model with axial fuel zones.

Numerical

The numerical model for the MCB simulation was limited to the geometry of the 17G fuel assembly. The initial core loading and subsequent reloading patterns were not reported in Ohi-2 experiment specification and thus the accurate reconstruction of the irradiation environment in the adjacent assemblies was impossible. Instead, the numerical model was surrounded by the reflective boundary conditions, which in a good way approximates the full core calculation. The bottom and top reflector below and above fuel rods were reconstructed as a homogenous mixes of structural materials and water coolant – see Fig. 4. The movement of AIC[3)] control rod cluster assemblies was not modeled because the in-core positions of the 17G fuel assembly does not correspond to any position reserved for control rod operation. The concentration of boric acid H_3BO_3 in cooling water for reactivity compensation was reconstructed using available data from Ohi-2 experiment specification.

The geometry of fuel rods and other elements installed in the fuel assembly were transferred to the 3D heterogeneous geometry of the computational model. The octal symmetry of the assembly allows fuel division into zones containing symmetrical sets of fuel rods. The numerical results in each individual symmetrical fuel rod would be the same due to aforementioned symmetry of the fuel assembly. The division reduced the complexity of the numerical model and associated computational time without loss of significant information. In total, the fuel was numerically divided into 84 fuel zones – 6 radial and 4 axial, as it is shown in Figs. 4 and 5. The cut fuel samples were represented by four fuel zones of 20 cm height located in the specified sets of fuel rods. Samples 89G03 and 89G05 were located in the same burnup zone, but they were differentiated by the FIMA burnup.

[3)] Silver-indium-cadmium alloy (80 wt% Ag, 15 wt% In, 5 wt% Cd).

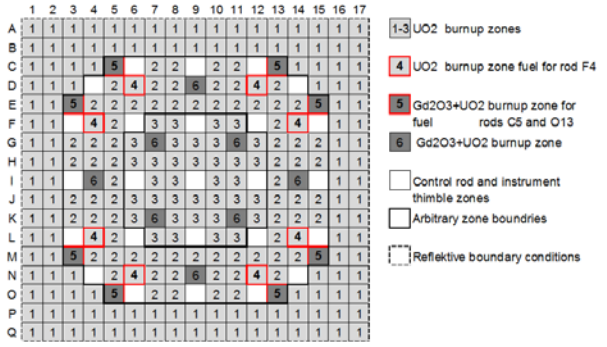

Fig. 5. Horizontal cross cut of the numerical model with six radial burnup zones.

The two-step calculation procedure includes one general burnup run for whole fuel assembly and five additional runs for adjustment of FIMA burnup in each fuel sample. The first run was normalized to the fuel assembly thermal power of 16.94 MW_{th} derived using average burnup of 31.5 GWd/t and initial FA fuel load of 451.76 kg. In additional runs, the FIMA burnup of the fuel zones representing fuel samples was adjusted to the measured FIMA burnup somewhat manipulating irradiation time. The simulations were performed for $7 \cdot 10^6$ particle histories at the each of 33 time points in the *kcode* mode. The large number of particle histories guarantees high precision for scoring function used for estimation of neutron fluxes and power – their relative error does not exceed 0.5%.

In order to reconstruct the behavior of the fissionable system, five sets of nuclear data libraries representing the best available knowledge about the particle interactions with the matter and natural nuclide properties were linked to the MCB code:

- JEFF3.1 continuous neutron transport cross-section libraries for 381 isotopes [10];
- decay schemas for about 2400 nuclides from the Table of Isotopes 8E [11] and dose data for about 738 nuclides from the Euroatom Council Directive 96/29/EUROATOM [12];
- one-group cross-section libraries previously applied in the ORIGEN code containing energy-integrated ratios of the nuclide formation in excited state due to the neutron capture, (n,2n) reaction and nuclear decay [13];
- branching ratios to the ground and metastable state in the function of the incident neutron energy for Am-242m and Am-244m based on the Mann and Schenter's evaluation [14];
- the incident energy depended fission products yields for 36 nuclides based on Wahl model [15].

Results

Uranium

Figure 6 shows time evolution of lumped uranium containing uranium isotopes present in the initial composition of the nuclear fuel, that is, U-234, U-235, U-236, and U-238. Evolutions for samples 89G03 and 89G05 are depicted as the same curve because in the numerical model the samples are

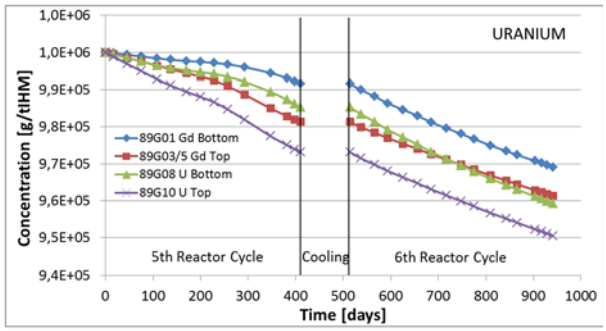

Fig. 6. Time evolutions of uranium.

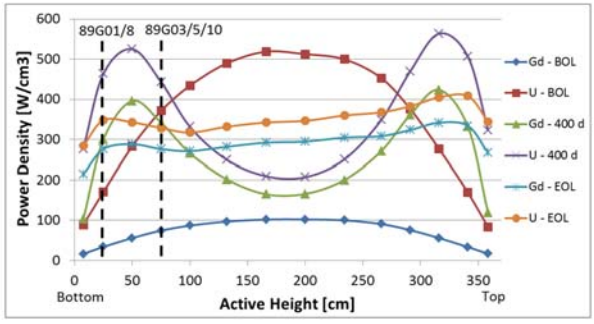

Fig. 7. Time evolution of axial power density for gadolinia bearing and pure uranium axial fuel zones.

located in the same fuel zone but differentiated by the FIMA burnup. The shape of the curves depends on the depletion of the most abundant uranium isotopes – U-235 and U-238. The concentration of U-235 mainly decreases due to fission while that of U-238 due to transmutation to higher actinides. The remaining uranium isotopes (e.g. U-232) produced in the consecutive chains of transmutations and decays do not influence time evolutions due to their small concentrations.

Table 6 quantifies the depletion of lumped uranium as well as of U-235 and U-238 for all fuel samples at specified FIMA burnup. In general, the lower depletion of 5–6% was observed for the gadolinium bearing samples. The reason for this is the initial presence of absorbing Gd-155/157 and lower macroscopic fission cross section due to lower concentration of U-235. The pure uranium samples 89G08/10 present the deeper depletion of 7–8%. Moreover, the axial location of the samples significantly influences the depletion of uranium – the larger depletion occurred in the top samples 89G03/5 and 89G10. This originates from the higher initial exposure to the neutron flux and thus larger neutron fluence in the regions located closer to center of the reactor core. The depletion rate increases after about 250 EFPD for all samples, which is caused by the changes in the neutron flux axial distribution from cosine shape to the two-hump shape and finally to the flat distribution. The neutron flux redistribution is influenced by two integrated effects: burnout of absorbing Gd-157/155 and depletion of fissile U-235. Figure 7 shows the redistribution of axial power density, which is directly proportional to the neutron flux. In the second irradiation cycle, uranium depletes almost in the linear manner for all samples because the axial neutron flux distribution does not change significantly. The decrease in uranium mass in the whole fuel sub-assembly during irradiation equals 4.5%, which corresponds to 20 kg.

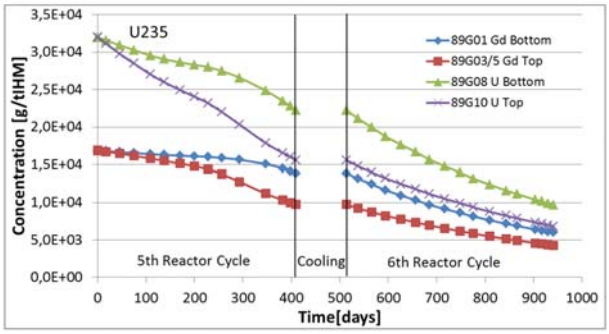

Fig. 8. Time evolutions of plutonium.

Plutonium

Plutonium isotopes are formed in the series of nuclear transmutation and decay chains starting from the neutron capture on U-238 and are not present in the initial fuel composition. Figure 8 shows the evolution of lumped plutonium containing Pu-236, Pu-238–Pu-242 in all investigated fuel samples. As it is shown, production of plutonium depends solely on the type of the sample – Gd bearing or pure uranium. However, it strongly depends on the axial location in the reactor core and thus on the neutron fluence. Therefore, the largest plutonium buildup was attained in the top samples 89G03/5 and 89G10. The plutonium evolutions depend on the neutron flux axial distribution similar to uranium, which is especially observable at 250th EFPD for bottom samples 89G01 and 89G08. At this point plutonium production rate begin to increase because of increasing absolute neutron flux. In the 6th reactor cycle, plutonium production rate increases faster for bottom samples, which corresponds to the higher absolute neutron flux. The total mass of plutonium in the fuel assembly at the end of 6th reactor cycle equals 4.4 kg, where mass of fissile Pu-239 shows

Table 6. Depletion of U-235 and U-238 obtained in MCB modeling

Sample	Type	FIMA [%]	Location [cm]	Initial concentration [g/tIHM]		Final concentration [g/tIHM]		Depletion [%]		
				U-235	U-238	U-235	U-238	U-235	U-238	Total
89G01	Gd_2O_3 + UO_2	2.211	26.7	1.69E+04	1.00E+06	5.76E+03	9.60E+05	66	4	5
89G03		2.950	73.7	1.69E+04	1.00E+06	3.94E+03	9.53E+05	77	5	6
89G05		2.585	73.3	1.69E+04	1.00E+06	4.77E+03	9.57E+05	72	4	5
89G08	UO_2	3.129	26.5	3.20E+04	1.00E+06	9.59E+03	9.46E+05	70	5	7
89G10		3.980	73.8	3.20E+04	1.00E+06	6.43E+03	9.38E+05	80	6	8

Table 7. C/E ratios for major actinides

Sample	89G01	89G03	89G05	89G08	89G10
Type	Gd	Gd	Gd	U	U
Location [cm]	26.7	73.7	73.3	26.5	73.8
FIMA [%]	2.211	2.950	2.585	3.129	3.981
Isotope			C/E		
U-232	0.12	0.13	0.11	0.82	1.04
U-234	1.00	1.01	1.00	1.00	0.99
U-235	1.05	1.08	1.08	1.05	1.05
U-236	1.01	1.00	0.99	0.99	0.99
U-238	1.00	1.00	1.00	1.00	1.00
Pu-236	1.54	1.28	1.29	1.32	1.20
Pu-238	0.97	0.95	0.96	0.92	0.95
Pu-239 + Np-239	1.01	0.99	1.00	1.01	1.00
Pu-240	1.02	1.00	1.00	1.01	0.98
Pu-241	1.01	0.99	0.99	0.99	0.99
Pu-242	1.03	0.98	0.97	0.99	0.97

the largest contribution of 2.5 kg. The formation of Pu-239 is extremely important for the core performances due to its high fission cross section in thermal energy range. The concentration of Pu-239 is usually reported together with concentration of Np-239 because of its short half-life time of 2.4 days.

Comparative analysis

The main results of the comparative analysis are presented in the form of the calculated-to-experimental ratios – C/E, which in the straight-forward manner indicate difference between calculations and measurements. The C/E ratios for all major actinides are presented in Table 7. We assume that C/E ratios in the range of 0.95–1.05 (±5%) correspond to the good agreement, which is satisfactory for the comparative analysis.

The good agreement was obtained for 43 matches out of 55 which correspond to about 78% of the results. The result previously published by Suyama *et al*. for the same benchmark specification but using different methodology based on the SWAT code, shows good agreement for 36 matches (65%) [2]. Hence, the results of MCB modeling in the more accurate way reflect the physics of the 17G fuel assembly. Among the investigated fuel samples the best results were obtained for the top uranium sample 89G10 – 10 matches out of 11 (91%) and for bottom gadolinia sample 89G01 – 9 matches out of 11 (82%). The remaining three samples indicate similar agreement of 8 matches out of 11 (73%). Considering C/E ratios for the individual isotopes, the results for U-235 for samples 89G03 and 89G05, as well as for Pu-238 for sample 89G03, exceed slightly the threshold of the good agreement by 3%. However, the C/E factors for Pu-236 and U-232 present large discrepancies[4)] unacceptable from the point of view of the numerical modeling.

Table 8 compares actinide concentrations obtained using MCB methodology and SWAT meth-

[4)] Apart from C/E for U-232 for sample 89G10.

Table 8. Comparison between MCB and SWAT methodology

Sample	89G01	89G03	89G05	89G08	89G10
Type	Gd	Gd	Gd	U	U
Location [cm]	26.7	73.7	73.3	26.5	73.8
FIMA [%]	2.211	2.950	2.585	3.129	3.981
Isotope			C_{MCB}/C_{SWAT}		
U-232	0.86	0.87	0.79	0.85	0.88
U-234	0.98	0.99	0.99	0.97	0.96
U-235	1.02	1.03	1.03	1.01	1.01
U-236	1.01	1.01	1.00	1.00	1.00
U-238	1.00	1.00	1.00	1.00	1.00
Pu-236	1.12	0.98	1.01	1.09	1.01
Pu-238	1.10	1.10	1.13	1.10	1.12
Pu-239	1.03	1.00	1.03	1.02	1.01
Pu-240	1.04	1.04	1.04	1.04	1.01
Pu-241	1.02	1.01	1.01	1.02	1.01
Pu-242	1.06	1.05	1.04	1.09	1.07

odology. The comparison between results attained using various numerical tools serves to detect discrepancies between applied numerical methodologies and helps to trace possible measurement errors. The reason for differences between both numerical tools is difficult to define and needs direct collaboration between scientific teams at the time of research. Therefore, we do not trace direct sources of discrepancies but use the results to verify the quality of the experimental measurements.

In the next two sections we investigate the behavior of the isotopes showing the largest discrepancies comparing with the experimental measurements, that is, U-232, U-235, Pu-236, and Pu-238.

U-235

In the fresh UOX fuel U-235 is the primary fissile isotope. The exposure to neutron flux gradually decreases U-235 concentration in two main nuclear processes: fission and neutron capture to U-236. The U-235 evolutions during both irradiation cycles are shown in Fig. 9. In the first irradiation cycle the U-235 evolutions for both sample types present unstable behavior caused by mentioned redistribution of the axial neutron flux. The effect influences U-235 depletion till about 250 EFPD, when the curves start to decrease in exponential manner. The 104 day interim cooling does not influence U-235 concentrations because of its long half-life of $7 \cdot 10^8$ years. In the second irradiation cycle U-235 concentration for all samples drops in exponential manner, which should happen in the absence of gadolinia burnable poison [16]. At the end of irradiation, the highest depletion was observed for the top pure uranium fuel sample 89G10 and the lowest for bottom gadolinia fuel sample 89G01, which of course corresponds to the largest and lowest FIMA burnup – see Table 6.

The U-235 concentrations obtained in MCB modeling shows overestimation of 5–8% when comparing it with experimental measurements. The similar overestimation but in the range of 3–5% was presented by Suyama *et al*. [2] which indicates to some inconsistencies in the benchmark specification. The most probable reasons for the U-235 overestimation might be:

– erroneous measurements of reference U-235 concentrations – the overestimation in U-235 concentrations was observed for MCB and SWAT modeling,

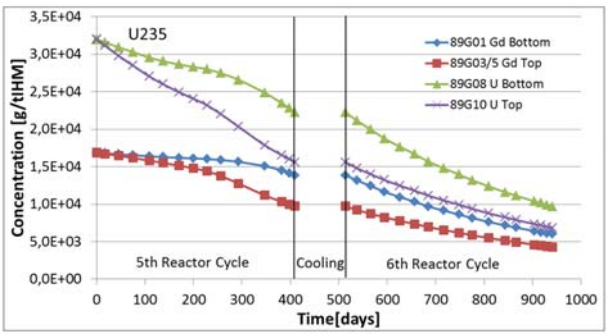

Fig. 9. Time evolutions of U-235.

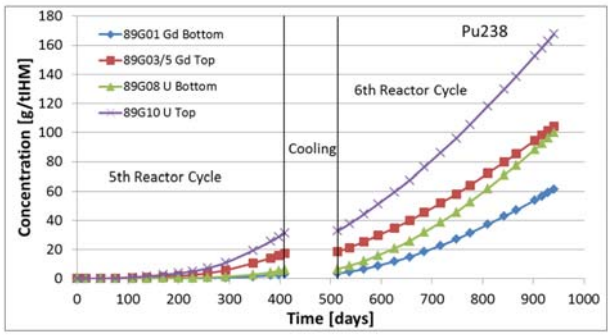

Fig. 10. Time evolutions of Pu-238.

– improper sample burnup estimation using Nd-148 method [17],
– error in the initial fuel density – the density in unit g/cm^3 was not reported, only theoretical density of 0.95 was known.

Pu-238

Pu-238 is mainly produced in the neutron capture on Np-237 and following β^- decay of Np-238 with half-life time of 2.1 days, as well as in α-decay of Cm-242 with half-life time of 160 days. The main removal channel of Pu-238 is neutron capture leading to the formation of Pu-239 and α-decay to U-234 with half-life time of 87.7 years. According to Fig. 10 the top fuel samples 89G03/5 and 89G10 present larger concentration of Pu-238 then bottom samples 89G01/8. This is attributed to the larger absolute neutron flux closer to reactor centerline. Generally, the gadolinia bearing samples show lower concentration of Pu-238 because of the lower concentration of U-238 and thus lower production of higher actinides. The Pu-238 concentration during interim outage increased on average about 6% due to decay of its precursor, especially Cm-242. The final mass of Pu-238 in fuel assembly equals 62 g.

The concentrations of Pu-238 for MCB as well as for SWAT calculations are underestimated, which gives C/E factors below unity. The differences for MCB equal from 3 to 8% while for SWAT are much larger – from 12 to 16%. The general improvement of the C/E factor in the MCB modeling indicates the numerical source of underestimation of Pu-238 concentrations rather than measurement error. The reason might lay in the aberration of production and destruction channels of higher actinides determining formation of Pu-238 precursors like Np-237 and Cm-242. Moreover, the sample 89G08 presents the largest underestimation for both calculations methodologies of 8 and 16%, respectively. It means that for this particular sample some measurement error could be deviated by final Pu-238 concentration. The C/E factors for remaining four samples: 89G01/3/5/10 present values in the range of good agreement.

U-232 and Pu-236

The concentrations of U-232 and Pu-236 are seldom reported and investigated because the relevance of

these isotopes for the radiological safety and waste management are negligible due to their very low concentrations in the reactor core [18]. One of the main sources of U-232 is the α-decay of Pu-236 with half-life time of 2.9 y, thus we show the behavior of both isotopes in the same section. The U-232 is removed either in α-decay to Th-228 with half-live time of 69 y or in neutron absorption. Pu-236 is mainly produced in β^- decay of Np-236m with half-life time of 22.5 h and removed in fission and neutron capture to Pu-237. The top uranium sample 89G10 shows the largest U-232 and Pu-236 final concentrations while gadolinia bottom sample 89G01 the lowest ones. This originates from the higher initial concentration of U-238 in pure uranium samples and thus larger macroscopic absorption cross section as well as from aforementioned axial neutron flux redistribution. The final concentrations of Pu-236 and U-232 show similar order of magnitude and equality at the end of irradiation in whole fuel assembly $5.6 \cdot 10^{-4}$ g and $1.5 \cdot 10^{-4}$ g, respectively.

The calculated final concentrations of U-232 for gadolinia bearing fuel samples 89G01/03/05 are much lower than concentrations obtained in experimental measurements, which results in the C/E ratios from 0.11 to 0.15. The large underestimation is recognized for the MCB and SWAT calculations. Therefore, either the concentrations obtained in the numerical simulations are too low or the measured concentrations are too large. It is remarkable that the measured concentrations of U-232 are larger in the gadolinia bearing fuel samples compared with the pure uranium samples, which is shown in Table 7. According to the calculated time evolutions of U-232 in Fig. 11, the gadolinia bearing samples should present about order of magnitude lower final concentrations – the measurements showed opposite results. In addition, the measured amounts of U-232 in the samples are very small, order of magnitude being 10^{-3} g/tIHM, which could have deviated experimental measurements. All these factors indicate high probability of measurement error for this particular isotope. The U-232 in uranium samples 89G08/10 behaves in different ways and present better agreement, especially for top uranium sample 89G10. The analysis of the bottom uranium sample 89G08 still shows large underestimation of 18%, which could be partly explained by the large measurement error of 7%. Additionally, the final concentrations of the Pu-236 are highly overestimated for all calculations and samples, while concentrations

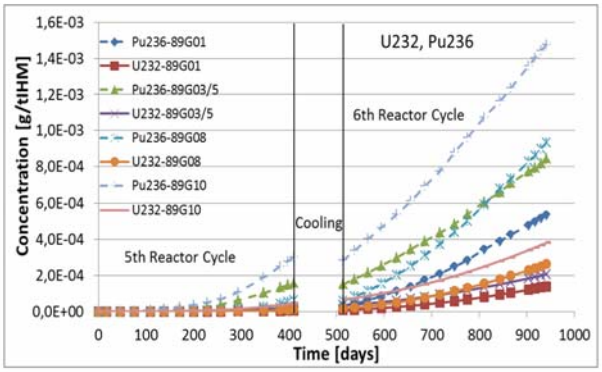

Fig. 11. Time evolutions of U-232 and Pu-236.

of U-232 for gadolinia bearing samples are strongly underestimated. In the numerical modeling, due to a high overestimation of Pu-236, the production of U-232 should be also overestimated. This is not true comparing C/E ratios for the gadolinia bearing samples and proves that the measurements of U-232 concentrations are erroneous and question the quality of the measured U-232 concentrations for the pure uranium samples. Moreover, the Pu-236 concentrations obtained using MCB and SWAT show perfect agreement for top samples. However, in the bottom samples, MCB modeling present large overestimation of about 10%. This, in a straightforward way indicates the influence of applied numerical setup on the final actinide concentrations.

Conclusions

The new methodology based on the MCB code was developed for the comparative analysis of measured and computed final concentrations of major actinides obtained in the Ohi-2 PWR irradiation experiment. The final concentrations of major actinides obtained in burnup calculations present good agreement of ±5% for 43 out of 55 C/E, which gives consistency of 78%. The poorest agreement was obtained for the U-232, U-235, Pu-236, and Pu-238. The U-232 and Pu-236 are not classified as isotopes important for the radiological safety or nuclear waste management. Thus, their concentrations are significant rather from the scientific not commercial point of view. The strong underestimation in Pu-238 occurred only for the one fuel sample 89G08. However, MCB as well as SWAT simulation shows the largest underestimation exactly for this sample. Hence, with high probability it can be attributed to the measurement error. The overestimation in U-235 is not acceptable for the detailed burnup calculations and its exact source should be defined in the further studies on Ohi-2 PWR benchmark specification. In general, the obtained results show that MCB code in the proper way reflects the physics of the investigated nuclear system. The high accuracy in estimation of major actinide concentrations encourages the usage of the MCB code in the applications related to the design and operation of the commercial nuclear systems.

The performed numerical analysis indicated some areas for improvement in the developed methodology and MCB code itself. First, the broader comparative analysis containing C/E ratios for minor actinides and some fission product would be helpful to describe detailed behavior of the 17G fuel assembly. Second, the MCB code should be equipped in the modules for the uncertainty and sensitivity analysis for quantification of the final uncertainties of C/E factors. The second task is more complex and can be solved by the means of perturbation theory developed initially in quantum mechanics. Last, the parallel execution of the MCB code can be significantly simplified using the RIMROCK [19] utility developed in the frame of the PL GRID NG project [20]. The research in all areas has already begun.

Abbreviations

AGH – Akademia Górniczo-Hutnicza
AIC – silver-indium-cadmium alloy
ASME – American Society of Mechanical Engineers
BOL – beginning of life
EFPD – effective full power day
EOL – end of life
FA – fuel assembly
FR – fuel rod
GEN-IV – Generation IV nuclear reactors
JAERI – Japan Atomic Energy Research Institute
JEFF – Joint Evaluated Fission and Fusion
KEPCO – Kansai Electric Power Company Inc.
MCB – The Monte Carlo continuous energy burnup code
MCNP – A general Monte Carlo n-particle transport code
PWR – pressurized water reactor
SWAT – step-wise burnup analysis code
TTA – transmutation trajectory analysis code
UOX – uranium dioxide fuel

References

1. Cetnar, J., Gudowski, W., & Wallenius, J. (1999). MCB: A continuous energy Monte Carlo burn-up simulation code. In Proceedings of Actinide and Fission Product Partitioning and Transmutation. (EUR 18898 EN, OECD/NEA 523).
2. Suyama, K., Murazaki, M., Ohkubo, K., Nakahara, Y., & Uchiyama, G. (2011). Re-evaluation of assay data of spent nuclear fuel obtained at Japan Atomic Energy Research Institute for validation of burnup calculation code systems. *Ann. Nucl. Energy*, *38*, 930–941. DOI: 10.1016/j.anucene.2011.01.025.
3. http://www.kepco.co.jp
4. Franceschini, F., & Petrović, B. (2009). Fuel with advanced burnable absorbers design for IRIS reactor core: Combined Erbia and IFBA. *Ann. Nucl. Energy*, *36*, 1201–1207. DOI: 10.1016/j.anucene.2009.04.005.
5. http://www.jaea.go.jp
6. Adachi, T., Nakahara, Y., Kohno, N., Gunji, K., Suzuki, T., Sonobe, T., Onuki, M., Kato, K., & Tachikawa, E. (1994). Comparison of calculated values with measured values on the amount of TRU and FP nuclide accumulated in gadolinium bearing PWR spent fuels, *J. Nucl. Sci. Technol.*, *31*(10), 1119–1129.
7. American Society for Testing and Materials. (2012). *Standard Test Method for Atom Percent Fission in Uranium and Plutonium Fuel (Neodymium-148 Method)*. U.S.A. (ASTM E321-96).
8. X-5 Monte Carlo Team. (2003). *MCNP-A General Monte Carlo N-Particle Transport Code*, *Version 5*. Los Alamos National Laboratory. (LA-UR-03-1987).
9. Cetnar, J. (2006). General solution of Bateman equations for nuclear transmutations. *Ann. Nucl. Energy*, *33*, 640–645. DOI: 10.1016/j.anucene.2006.02.004.
10. Koning, A., Forrest, R., Kellett, M., Mills, R., Henriksson, H., & Rugama, Y. (2006). *The JEFF-3.1 Nuclear Data Library*. OECD Nuclear Energy Agency. (OECD JEFF Report 21).
11. Firestone, R., Shirley, V., Baglin, C., Chu, S., & Zipkin, J. (1996). *Table of Isotopes 8E*. New York: John Wiley & Sons, Inc.
12. IAEA. (1996). *The Basic Safety Standards*. Vienna: International Atomic Energy Agency. (Safety Series No. 115).
13. Croff, A. (1980). *A User's Manual for the ORIGEN2 Computer Code*. Oak Ridge National Laboratory. (ORNL/TM 7157).
14. Mann, F., & Schenter, R. (1977). Calculated neutron capture cross sections to the americium ground and isomer states. *Nucl. Sci. Eng.*, *63*, 242–249.
15. Wahl, A. (1985). Nuclear-charge distribution near symmetry for thermal-neutron-induced fission of ^{238}U. *Phys. Rev. C*, *32*, 184–195.
16. Canadian Nuclear Safety Commission. (2003). *Reactor physics*. CNSC Science and Reactor Fundamentals – Reactor Physics Technical Training Group.
17. Lewins, J., & Becker, M. (2002). *Advances in nuclear science and technology* (Vol. 25). New York: Kluwer Academic Publishers.
18. OECD Nuclear Energy Agency. (2011). *Spent nuclear fuel assay data for isotopic validation*. (Nuclear Science NEA/NSC/WPNCS/DOC(2011)5).
19. Harężlak, D., Kasztelnik, M., & Pawlik, M. (2015). *RIMROCK Robust Remote Process Controller*. Retrieved 21 March 2015, from https://submit.plgrid.pl/
20. Konsorcjum PL-Grid. (2015). Retrieved 21 March 2015, from http://www.plgrid.pl/projekty/ng.